Published in final edited form as:
Brain Res. 2010 October 1; 1354C: 179–187. doi:10.1016/j.brainres.2010.07.040.

Luminal platelet aggregates in functional deficits in parenchymal vessels after subarachnoid hemorrhage

Victor Friedrich, Ph.D[2], **Rowena Flores, MD**[1], **Artur Muller, M.S**[1], and **Fatima A. Sehba**[1,2]
[1]Department of Neurosurgery, Mount Sinai School of Medicine, New York, NY 10029
[2]Department of Neuroscience, Mount Sinai School of Medicine, New York, NY 10029

Abstract

The pathophysiology of early ischemic injury after aneurysmal subarachnoid hemorrhage (SAH) is not understood. This study examined the acute effect of endovascular puncture-induced SAH on parenchymal vessel function in rat, using intravascular fluorescent tracers to assess flow and vascular permeability and immunostaining to assess structural integrity and to visualize platelet aggregates. In sham-operated animals, vessels were well filled with tracer administered 10 seconds before sacrifice, and parenchymal escape of tracer was rare. At ten minutes and 3 hours after hemorrhage, patches of poor vascular filling were distributed throughout the forebrain. Close examination of these regions revealed short segments of narrowed diameter along many profiles. Most vascular profiles with reduced perfusion contained platelet aggregates and in addition showed focal loss of collagen IV, a principal component of basal lamina. In contrast, vessels were well filled at 24 hours post-hemorrhage, indicating that vascular perfusion had recovered. Parenchymal escape of intravascular tracer was detected at 10 minutes post-hemorrhage and later as plumes of fluorescence emanating into parenchyma from restricted microvascular foci. These data demonstrate that parenchymal microvessels are compromised in function by 10 minutes after SAH and identify focal microvascular constriction and local accumulation of luminal platelet aggregates as potential initiators of that compromise.

Classification terms

Section; Disease-Related Neuroscience

Keywords

stroke; aneurysmal subarachnoid hemorrhage; parenchymal vessels; perfusion; permeability

Introduction

Aneurysmal subarachnoid hemorrhage (SAH) is accompanied by early cerebral ischemic injury and high 48 hour mortality (Bederson et al., 1998; Gewirtz et al., 1999; Stoltenburg-

Corresponding and proofs to Fatima A. Sehba, PhD, Departments of Neurosurgery and of Neuroscience, Box 1136, Mount Sinai School of Medicine, New York, NY 10029, USA. Fax: 212 241 0697, Phone: 212 241 6504, fatima.sehba@mssm.edu.

Didinger and Schwartz, 1987). The mechanisms of early ischemic injury are poorly understood and specific treatment options are limited.

Recently attention has turned to the cerebral parenchymal vessel as a possible site of early ischemic injury after SAH (Ishikawa et al., 2009; Scholler et al., 2007; Sehba and Bederson, 2006; Yatsushige et al., 2007). Structural changes in parenchymal microvessels sufficient to affect their function are found as early as 10 minutes after SAH. These include microvascular constriction, focal accumulation of luminal platelet aggregates (Sehba et al., 2005), detachment of endothelium lining, the appearance of gaps in the collagen IV-immunoreactive basal membrane, and transmigration of platelets or platelet aggregates into brain parenchyma (Friedrich et al., 2010; Sehba et al., 2004; Sehba et al., 2005; Sehba et al., 2007). These observations indicate that rapid and dramatic changes in structure of brain microvessels occur following SAH, but do not directly address the relationship between these events and perfusion and permeability. The current study combines intravascular tracer analysis with immunostaining and three-dimensional visualization to visualize disturbances in perfusion and permeability and to relate them to structural changes described previously.

Results

Microvascular perfusion

FITC-dextran vascular labeling—Fixable FITC-dextran was injected intrafemorally 10 seconds before sacrifice. In sham-operated controls, the tracer filled the cerebral vasculature (Figure 1A) and labeled vessels were uniformly distributed across the two hemispheres and across brain regions (basal, frontal, and convexity cortex, and striatum). The right-left symmetry of labeling demonstrates that brief (unilateral) introduction of the monofilament into the ICA, without induction of hemorrhage, does not cause perfusion deficits.

By contrast, in SAH animals pale and bright vascular patches of poor and well filled fluorescent label were present (Figure 1A). These patches exhibited no specific anatomical pattern and were present in both hemispheres and in all brain regions. At high magnification pale patches showed little vascular fluorescence, indicating substantially reduced rate of perfusion. In contrast, a substantial amount of fluorescence was present in the brighter, better-perfused patches (Figure 1B). Patches of poor perfusion were evident at 10 minutes post-hemorrhage (not shown) and prevalent at 3 hours post-hemorrhage (Figure 1A). At 24 hours post-hemorrhage, vessel filling had substantially improved (Figure 1A). These patches of poor perfusion were absent at all survival intervals from sham-operated specimens, indicating that impaired perfusion resulted neither from surgery without hemorrhage nor from the procedure used for injecting vascular tracer but rather from the subarachnoid hemorrhage and its sequellae.

We determined the area fraction of FITC-dextran positive vascular profiles in our images as a rough quantitative index of vascular perfusion. This index was significantly reduced at 10 minute and 3 hours post-hemorrhage and increased at 24 hours in comparison to sham-operated animals (Figure 1B). In addition, we determined the average vascular diameter in sham and SAH animals (Figure 1C). The data showed no significant change in the vascular diameter at 10 minutes, a small but significant decrease at 3 hours ($P=0.003$), and small but significant increase (dilation) at 24 hours post hemorrhage.

FITC-dextran and platelet immunostaining—To assess the relationship between vascular perfusion and luminal platelet aggregates, we immunostained brain sections of animals sacrificed 3hours after SAH for platelet-specific antigen. As reported previously, a large number of parenchymal vessels contained luminal platelet aggregates (Sehba et al., 2005). Under low magnification these aggregates appeared as red dots in otherwise green

fluorescent vascular profiles. In high magnification two kinds of vascular segments could be identified; segments that contained little FITC-dextran label and were filled with platelet aggregates; indicates mechanical obstruction in flow and segments with decreased diameter filled with platelet aggregates and FITC-dextran; indicates local constriction (Figure 2). In addition, many continuous FITC-dextran label vascular profiles appeared to be interrupted such that they terminated for a brief (approximately 5um) distance and then continued. Platelet staining was always found at the edges of the interrupted segments (Figure 2).

Microvascular Permeability

FITC-Albumin extravasation—To assess blood-brain barrier function, we injected animals intrafemorally with FITC-albumin and sacrificed them 15 minutes later by vascular perfusion with saline followed by a formaldehyde fixative. The perfusion cleared most of the intravascular FITC-albumin, leaving extravascular FITC which marked sites where albumin had escaped from the vasculature. Sections were also immunostained for collagen-IV to visualize the microvascular basal lamina. Little extravasation was evident in sham-operated animals, indicating that the blood-brain barrier was intact after sham surgery. By contrast in SAH animals approximately 20% collagen IV positive parenchymal vessel profiles were associated with small accumulations of extravascular FITC-albumin. These foci of extravasation were visible in 10 minutes, 3 hours and 24 hours post-hemorrhage specimens, in all brain regions and in both hemispheres. High magnification, 3D confocal microscopy showed small windows in collagen IV immunofluorescence near the vascular sites of extravasation (Figure 3A). Much of the extravasated FITC-albumin was located in the parenchymal cells; indicates active phagocytosis (Figure 3B). To quantitate extravasation, the number of vessels with FITC-albumin extravasation was counted. A substantially greater number of vessels exhibited FITC-albumin extravasation at 10 minutes to 24 hours post-hemorrhage as compared to time matched sham cohorts (Figure-3C).

In addition to parenchyma, FITC-albumin fluorescence was also present in the lumen of vessels. In higher magnification vascular fluorescence was found to be located within luminal cells (Figure 3B). The number of these vascular cells decreased with time after SAH. No fluorescent cells were found in parenchymal vessels of sham–operated animals.

FITC-Albumin and platelet immunostaining—Most vessels with FITC-albumin extravasation contained luminal platelet aggregates. In some cases platelets appeared to be extravasating along with FITC-albumin into the parenchyma via an apparent shared vascular exit site (Figure-4).

Discussion

The present study examined functional alterations in parenchymal vessels after aneurismal SAH with a focus on the contribution of intraluminal platelet aggregates in these events. The results demonstrate that focal vasoconstriction, profound perfusion deficits, and permeability changes occur in parenchymal microvessels within minutes after SAH. These vascular changes are associated with accumulation of platelet aggregates, suggesting that intraluminal platelet aggregates may play a causative role in early microvascular compromise. This is the first report establishing disruption of microcirculation within minutes after SAH. It provides a foundation for the design and evaluation of therapies against the early injury after SAH.

Perfusion deficits after SAH

Reduced cerebral perfusion in the hours after SAH is established. These reduction is observed directly by laser Doppler flowmetry or indirectly by observing reduced partial filling of vasculature by injected intravascular tracers (such as carbon black, Evans blue, etc (Bederson

et al., 1995; Hertel et al., 2005; Schubert et al., 2008; Vajkoczy et al., 2003; Westermaier et al., 2009). In the present study, we injected a high molecular weight Dextran into the peripheral circulation and sacrificed animals 10 seconds later. The high molecular weight was chosen to limit the extravasation of tracer from intact vessels. The very short time allowed between injection of tracer and sacrifice was just sufficient to allow filling of un-obstructed, patent vessels, while vessels with reduced perfusion filled only partially. Hence, in naïve and in sham operated animals 10 seconds circulation fills cerebral vasculature with tracer completely (Figure-1A).

Using this technique we found substantial reduction in vascular filling at 10 minutes after SAH, continuing beyond 3 hours post-hemorrhage. Our results are consistent with previous studies showing perfusion deficits in parenchymal vessels and capillaries one hour after SAH (Trojanowski, 1984) but show further that reduced perfusion begins within minutes after SAH. We find further that, at that earliest survival time, perfusion deficits mainly reside in those microvessels which contain platelet aggregates. It should be noted that the obstruction of vessel lumens by lodged platelet aggregates could in itself reduce or block flow. In addition, vasoactive compounds and thrombin released by activated platelets and injured endothelium are known to promote local vasoconstriction (Fukami et al., 2001; Levin, 1995). Constricted segments of otherwise normal vessels were indeed frequently observed and were mostly located next to the platelet aggregates, suggesting that lodging of platelet aggregates might either initiate local vasoconstriction or potentiate constriction already in progress.

Permeability deficits and platelets

Compromise of the blood-brain barrier after SAH is well known (Doczi et al., 1986; Scholler et al., 2007; Smith et al., 1997; Yatsushige et al., 2006). This phenomenon was previously documented 3 hours after the initial hemorrhage (Doczi et al., 1986); the present study demonstrates that extravasation of large molecules from microvessels begins within 10 minutes of hemorrhage. This result is consistent with those of our previous studies of this time point, which found focal loss of the blood-brain barrier antigen EBA (Sehba et al., 2007), loss of vascular basal lamina (Friedrich et al., 2010; Sehba et al., 2007), and extravasation of platelets (Friedrich et al., 2010). Taken together, the data indicate that platelet aggregation, structural compromise of microvessels, and functional compromise of the blood brain barrier occur within minutes post SAH and possibly represent key substrates for subsequent pathology. Other mechanisms posited as initiators of increased parenchymal vessel permeability after SAH include transient increases in ICP and BP and a decrease in cerebral perfusion pressure which occur at SAH (Zuccarello et al., 1987), compression by the blood clot (Johshita et al., 1990), attack by free radicals (Smith et al., 1997), and opening of inter-endothelial tight junctions (Doczi, 1985).

Potential mechanisms of platelet aggregation in microvessels after SAH

The initial activation of platelets may well occur at site of the aneurysm rupture (Kapp et al., 1968). The massive intravascular platelet aggregation which follows throughout the brain may result from the activity of pro-coagulants and vasoconstrictive agents released from degranulating platelets and injured endothelium (Akopov et al., 1996; Fujimoto et al., 1985), from expression of platelet-attracting integrin receptors on the parenchymal endothelium (Ishikawa et al., 2009), and/or from alterations in the NO/NOS pathway and reduction in cerebral NO early after SAH (Sehba et al., 2000) Under normal physiology NO, produced by endothelial cells and/or by platelets themselves, inhibits platelet adhesion and aggregation. Fall in cerebral NO after SAH will remove this feedback inhibition of platelet aggregation and stimulate platelet aggregation.

In conclusion, we here report profound perfusion deficits and permeability changes in parenchymal vessels within 10 minutes after SAH. Furthermore we find luminal platelet aggregates frequently located at the sites of early microvascular constriction, reduced perfusion, and extravasation of intravascular tracer. Although detailed mechanisms remain to be established, our findings suggest an embolic source of early vascular deficits. Platelet activation, aggregation and signaling may prove fruitful targets for therapeutic interventions against early ischemic injury after SAH.

Experimental procedure

All experimental procedures and protocols were approved by the Institutional Animal Care and Use Committee of the Mount Sinai Medical Center.

Animal model of aneurysmal subarachnoid hemorrhage

Male Sprague-Dawley rats (325–350g) underwent experimental SAH using the endovascular suture model (Bederson et al., 1995; Schwartz et al., 2000). Briefly, rats were anesthetized with ketamine-xylazine (80mg/Kg+10mg/Kg; IP), transorally intubated, ventilated, and maintained on inspired isoflourane (1% to 2% in oxygen-supplemented room air). Rats were placed on a homeothermic blanket Harvard Apparatus, MA, USA) attached to a rectal temperature probe set to maintain body temperature at 37°C and positioned in a stereotactic frame. The femoral artery was exposed and cannulated for blood gas and blood pressure (BP) monitoring (ABL5, Radiometer America Inc. Ohio, USA). Blood gases for experiments included in this study were mean ± sem; pO2: 137±1.0, pCO2: 38 ±0.7, pH: 7.3±0.006. For measurement of intracranial pressure (ICP), the atlanto-occipital membrane was exposed and cannulated, and the cannula was affixed with methymethacrylate cement to a stainless steel screw implanted in the occipital bone. Cerebral blood flow (CBF) was measured by laser-Doppler flowmetry, using a 0.8mm diameter needle probe (Vasamedics, Inc., St. Paul, MN, USA) placed directly over the skull away from large pial vessels in the distribution of the middle cerebral artery.

SAH was induced by advancing a suture retrograde through the ligated right external carotid artery, and distally through the internal carotid artery until the suture perforated the intracranial bifurcation of the internal carotid artery. This event was detected by a rapid rise in ICP and bilateral decrease in CBF. Animals were monitored from 20 minutes prior to SAH to 10 minutes or 3 hours after SAH. As animals regained consciousness and were able to breathe spontaneously they were returned to their cages and sacrificed at 10 minutes, 3 hours, or 24 hours after SAH.

Sham surgery consisted of all steps described above for the induction of SAH, including the introduction of the suture through the external to the internal carotid artery; however, artery was not perforated. In this study, sham-operated controls were matched in post-operative survival time to the SAH animals.

SAH Physiological Parameters

Animals were assigned randomly to survival interval and treatment groups (n=5–7 per time interval per surgery group). ICP, CBF and BP were recorded in the real time. Average ICP rise at SAH from baseline was: 5.5±0.5mmHg, peak: 64.8±8.4mmHg; CBF, fall at SAH to 15.8 ±2.0% and at 10 and 60 minutes recovered to 38.6±4.8% and 68.4±11.4% of baseline respectively; BP, unchanged after SAH. The ICP and CBF values indicated that rats experienced *moderate* SAH (Figure-1) (Bederson et al., 1998). 24 hour mortality after SAH and shams surgeries was 29% and 10%, respectively.

Microvascular perfusion by fluorescent tracer injection

The rat was sedated and femoral artery was cannulated. FITC-dextran (2×10^6 molecular weight, Sigma, St. Louis, MO) was injected interfemorally (bolus injection; 0.5ml of 50 mg/ml preparation; n=5–7 per time interval per surgery group). Ten seconds after the injection the rat was sacrificed by decapitation using guillotine. In preliminary experiments we have found that 10 seconds is enough time for tracer to fill parenchymal vessels of a naive animal completely.

Upon sacrifice brain was isolated and immersed in 4% PAF and then in solutions that were prepared in 4% PAF and contained 10%, 20% or 30% sucrose. Finally the brain was embedded in Tissue-Tek OCT compound (Miles, Elkhart, IN) and frozen in 2-methylbutane cooled in dry ice. Serial coronal brain sections 8 or 20μm thick were cut on a cryostat and thaw-mounted onto gelatin-coated slides. Sections located at bregma −8.0, +0.2 and +1.2 (Paxinos and Watson, 1986) are used for examining perfusion deficits. Sections were washed with PBS, coverslipped and observed by fluorescent and confocal microscopy. Images of whole coronal brain section (fluorescence microscopy) were analyzed for the presence of vascular tracer vascular presence of tracer using IPLab software (see below).

Microvascular permeability: FITC-albumin Extravasation

The rat was sedated and the femoral artery was cannulated. FITC-albumin (Sigma, St. Louis, MO) was injected 15 minute before sacrifice (bolus injection; 0.5ml of 20 mg/ml preparation, n=5 per time interval per surgery group). In preliminary studies we found that 15 minutes allowed sufficient extravasation for discrete sites of leaks to be visible in the microscope.

Animals were killed by means of transcardiac perfusion with chilled saline followed by 1% chilled PAF. This procedure washes blood and free tracer out of the vessel lumen and fixes tracer at the sites of parenchymal leaks. The brain was isolated and immersed in 1% PAF and then in solutions that contained 10%, 20% or 30% sucrose in 1% PAF. Immersion in each solution was carried over night at 4°C.

Finally, brain was embedded in Tissue-Tek OCT compound (Miles, Elkhart, IN), and frozen in 2-methylbutane cooled in dry ice and stored at −70°C until use. Serial coronal brain sections 8 μm thick were cut on a cryostat and thaw-mounted onto gelatin-coated slides. Sections located at bregma −8.0, +0.2 and +1.2 (Paxinos and Watson, 1986) were used for permeability study. These sections were washed with PBS, coverslipped, and observed by confocal microscopy. Images from three brain areas (striatum, basal and frontal cortex) were taken and analyzed for tracer leaks (see below).

Immunostaining

Immunoreagents—*Primary antibodies* were: rabbit polyclonal anti-collagen IV (Abcam, Inc, Cambridge, MA; cat. no AB6586); rabbit anti-rat platelets (Inter Cell Technologies Inc, Jupiter, FL; cat. no. ADG51440); and Texas Red-conjugated rabbit anti-rat platelets (Inter Cell Technologies). Secondary antibodies were: species-specific donkey anti-rabbit-Rhodamine Red-X (Jackson ImmunoResearch, West Grove, PA; cat. no. 711-295-152) and species-specific donkey anti-rabbit- DyLight 649 (Jackson ImmunoResearch; cat. no. 711-949-152). Unconjugated fab fragments of goat anti-rabbit antibodies (Jackson ImmunoResearch cat. no: 111-077-003) were used for blocking in dual collagen IV-platelets immunostaining.

Immunostaining procedures—Cryostat sections (8μm) from FITC-dextran and FITC-albumin injected animals were thawed, postfixed in 4% paraformaldehyde, washed in PBS, and blocked in a solution of 5% normal donkey serum in PBS (DB). For *single immunofluorescence*, sections were then incubated overnight at with either rabbit anti-collagen

IV (1:100 in DB) or rabbit anti-platelets (5μg/ml in DB), washed in PBS, incubated overnight at 4°C with donkey anti-rabbit-Rhodamine Red-X (15μg/ml in DB), washed in PBS, and coverslipped with Vectastain with or without DAPI (Vector labs, Burlingame, CA, USA). For *double immunofluorescence*, sections prepared as above were incubated with Texas Red-conjugated rabbit anti-rat platelets (5μg/ml in DB) overnight at 4°C, washed with PBS, incubated with unconjugated fab fragments of goat anti-rabbit antibodies (4.8μg/ml in DB) overnight at 4°C, washed with PBS followed by DB, incubated with rabbit anti-collagen IV (1:100 in DB) overnight at 4°C, washed with PBS, incubated with donkey anti-rabbit-DyLight 649 (15μg/ml in DB), washed in PBS, and coverslipped as above.

Data Acquisition

Physiology—CBF, ICP, and mean arterial blood pressure (MAP) data were continuously recorded starting 20 minutes before SAH and ending 10 or 60 minutes after SAH (PolyView software; Grass Instruments; MS, USA). CBF data were normalized to the baseline value averaged over 20 minutes prior to SAH, and subsequent values expressed as a percentage of baseline (Sehba et al., 1999).

Morphometry—Specimens were evaluated by an observer blinded to their identity. Vessels included in this study were 100um or less in diameter; these include pre- and post capillary arteries and venules. Moreover, no distinction between capillaries and venules was made. Quantitative analysis (perfusion deficits and changes in permeability and vascular diameter) was performed with IPLab software (IPLab v3.6.3, Signal Analytics). The area fraction and the diameter of FITC-dextran labeled vessels and count of collagen IV positive vessels with FITC-albumin leaks were determined.

Area fractions—Images of FITC-dextran labeled vessels were segmented by intensity thresholding accompanied by the profile size gating to select all visible tracer labeled vessel profiles. The program (IP lab) computed area fraction as the sum of segmented profiles in a field divided by the total area of the field. For each assay session a single slide selected in advance from the collection of sham operated animals was used to establish the thresholding parameters, which were then kept constant during the remainder of the session. The area fraction, a standard stereological measure, estimates the total amount of a partition as a fraction of total sample volume.

Vascular diameter—Vessels were segmented by intensity thresholding as above. The width of each vascular profile was estimated as the length of the minor axis of an ellipse fitted to the vascular profile (IPLab software; Scanalytic Inc, v 3.63; USA) (Sehba et al., 2007).

Vessel profile counts—Collagen IV-positive vessel profiles and FITC-albumin deposits visible in micrographs from basal and frontal cortex and striatum were counted manually by an observer blinded to specimen identity. Some material was also analyzed automatically using intensity threshold segmentation to select and count profiles (IPLAB). The results were consistent with those of manual counts; but the irregularity of escaping FITC-albumin deposits caused excessive variability and the automated count data were therefore not included in the study.

Microvascular Perfusion analysis—Composite montages of whole coronal brain sections were taken using an automated stage and Leica DM-600 microscope (5 × objective, NA: 0.15) were assembled using MetaMorph (Molecular Devices, CA, USA) and were studied for the area fraction and diameter of labeled vascular profiles using IP lab software (see above). Colocalization of FITC-dextran and platelets in frontal and basal cortex and striatum was studied via confocal microscopy (Leica SP5 DM). 3 D rendered stacked high magnification

confocal Z stacks were generated and vascular segments and areas of low perfusion with respect to the presence of local platelet aggregates were identified.

Microvascular Permeability—was studied in brain sections immunostained for collagen IV and platelets. Collagen IV immunostaining was used to delineate the microvasculature, to determine the number of leaky vessels, and to analyze leaky sites with respect to the vascular wall and local platelet aggregates. Confocal images Z stacks were generated and used for quantifying the vessels with leaks (see above). The presence of platelets and collagen IV around the site of FITC-albumin leak studied was identified using high resolution confocal images.

Statistical analysis

Each parameter (ICP, CBF, area fraction and the length and width of vascular profiles) was analyzed by ANOVA (StatView v 5.0.1, SAS institute Inc. USA) with time and treatment query (control, SAH). Pairwise comparison used Fisher's PLSD *post-hoc* tests.

Abbreviations

SAH	Subarachnoid hemorrhage
BP	blood pressure
ICP	intracranial pressure
CBF	Cerebral blood flow

Acknowledgments

This study was supported by supported by National Institutes of Health Grant No. RO1 NS050576 (F.A.S). Confocal and widefield microscopy were performed at the Mount Sinai School of Medicine Microscopy Shared Resource Facility.

Literature References

Akopov S, Sercombe R, Seylaz J. Cerebrovascular reactivity: role of endothelium/platelet/leukocyte interactions. Cerebrovasc Brain Metab Rev 1996;8:11–94. [PubMed: 9052980]

Bederson JB, Germano IM, Guarino L. Cortical blood flow and cerebral perfusion pressure in a new noncraniotomy model of subarachnoid hemorrhage in the rat. Stroke 1995;26:1086–1091. [PubMed: 7762027]

Bederson JB, Levy AL, Ding WH, Kahn R, DiPerna CA, Jenkins ALr, Vallabhajosyula P. Acute vasoconstriction after subarachnoid hemorrhage. Neurosurgery 1998;42:352–360. [PubMed: 9482187]

Doczi T. The pathogenetic and prognostic significance of blood-brain barrier damage at the acute stage of aneurysmal subarachnoid haemorrhage. Clinical and experimental studies. Acta Neurochir (Wien) 1985;77:110–132. [PubMed: 4072781]

Doczi T, Joo F, Adam G, Bozoky B, Szerdahelyi P. Blood-brain barrier damage during the acute stage of subarachnoid hemorrhage, as exemplified by a new animal model. Neurosurgery 1986;18:733–739. [PubMed: 3736802]

Friedrich V, Flores R, Muller A, Sehba FA. Escape of intraluminal platelets into brain parenchyma after subarachnoid hemorrhage. Neuroscience 2010;165:968–975. [PubMed: 19861151]

Fujimoto T, Suzuki H, Tanoue K, Fukushima Y, Yamazaki H. Cerebrovascular injuries induced by activation of platelets in vivo. Stroke 1985;16:245–250. [PubMed: 3975962]

Fukami, MH.; Holmsen, H.; Kowalska, MA.; Niewiarowski, S. Platelet Secretion. In: Colman, RW.; Hirsh, J.; Marder, VJ.; Clowes, AW.; George, JN., editors. Hemostatis and thrombosis basic principles and clinical practice. Vol. Vol.. Phialdelphia, PA, USA: Lippincott Williams & Wilkins; 2001. p. 562-573.

Gewirtz RJ, Dhillon HS, Goes SE, DeAtley SM, Scheff SW. Lactate and free fatty acids after subarachnoid hemorrhage. Brain Res 1999;840:84–91. [PubMed: 10517955]

Hertel F, Walter C, Bettag M, Morsdorf M. Perfusion-weighted magnetic resonance imaging in patients with vasospasm: a useful new tool in the management of patients with subarachnoid hemorrhage. Neurosurgery 2005;56:28–35. discussion 35. [PubMed: 15617583]

Ishikawa M, Kusaka G, Yamaguchi N, Sekizuka E, Nakadate H, Minamitani H, Shinoda S, Watanabe E. Platelet and leukocyte adhesion in the microvasculature at the cerebral surface immediately after subarachnoid hemorrhage. Neurosurgery 2009;64:546–553. discussion 553–4. [PubMed: 19240618]

Johshita H, Kassell NF, Sasaki T. Blood-brain barrier disturbance following subarachnoid hemorrhage in rabbits. Stroke 1990;21:1051–1058. [PubMed: 2368106]

Kapp J, Mahaley MS Jr, Odom GL. Cerebral arterial spasm. 2. Experimental evaluation of mechanical and humoral factors in pathogenesis. J Neurosurg 1968;29:339–349. [PubMed: 4301729]

Levin ER. Endothelins. N Engl J Med 1995;333:356–363. [PubMed: 7609754]

Paxinos, G.; Watson, C. The Rat Brain in Stereotaxic Coordinates. Vol. Vol.. San Diego, California: Academic Press Inc.; 1986.

Scholler K, Trinkl A, Klopotowski M, Thal SC, Plesnila N, Trabold R, Hamann GF, Schmid-Elsaesser R, Zausinger S. Characterization of microvascular basal lamina damage and blood-brain barrier dysfunction following subarachnoid hemorrhage in rats. Brain Res 2007;1142:237–246. [PubMed: 17303089]

Schubert GA, Poli S, Mendelowitsch A, Schilling L, Thome C. Hypothermia reduces early hypoperfusion and metabolic alterations during the acute phase of massive subarachnoid hemorrhage: a laser-Doppler-flowmetry and microdialysis study in rats. J Neurotrauma 2008;25:539–548. [PubMed: 18352824]

Schwartz AY, Masago A, Sehba FA, Bederson JB. Experimental models of subarachnoid hemorrhage in the rat: A refinement of the endovascular filament model. J Neurosci Methods 2000;96:161–167. [PubMed: 10720681]

Sehba FA, Ding WH, Chereshnev I, Bederson JB. Effects of S-nitrosoglutathione on acute vasoconstriction and glutamate release after subarachnoid hemorrhage. Stroke 1999;30:1955–1961. [PubMed: 10471450]

Sehba FA, Schwartz AY, Chereshnev I, Bederson JB. Acute decrease in cerebral nitric oxide levels after subarachnoid hemorrhage. J Cereb Blood Flow Metab 2000;20:604–611. [PubMed: 10724124]

Sehba FA, Mostafa G, Knopman J, Friedrich V Jr, Bederson JB. Acute alterations in microvascular basal lamina after subarachnoid hemorrhage. J Neurosurg 2004;101:633–640. [PubMed: 15481718]

Sehba FA, Mustafa G, Friedrich V, Bederson JB. Acute microvascular platelet aggregation after Subarachnoid hemorrhage. J Neurosurg 2005;102:1094–1100. [PubMed: 16028769]

Sehba FA, Bederson JB. Mechanisms of Acute Brain injury after Subarachnoid Hemorrhage. Neurol Res 2006;28:381–398. [PubMed: 16759442]

Sehba FA, Makonnen G, Friedrich V, Bederson JB. Acute cerebral vascular injury occurs after subarachnoid hemorrhage and can be prevented by administration of a Nitric Oxide donor. J Neurosurg 2007;106:321–329. [PubMed: 17410718]

Smith SL, Larson PG, Hall ED. A comparison of the effects of tirilazad on subarachnoid hemorrhage-induced blood-brain barrier permeability in male and female rats. J Stroke Cerebrovasc Dis 1997;6:389–393. [PubMed: 17895039]

Stoltenburg-Didinger, G.; Schwartz, K. Brain Lesions Secondary to Subarachnoid Hemorrhage due to ruptured aneurysms. In: Cervos-Navarro, J.; Ferst, R., editors. Stroke and Microcirculation. Vol. Vol.. New York: Raven Press; 1987. p. 471-480.

Trojanowski T. Early effects of experimental arterial subarachnoid haemorrhage on the cerebral circulation. Part II: Regional cerebral blood flow and cerebral microcirculation after experimental subarachnoid haemorrhage. Acta Neurochir 1984;72:241–255.

Vajkoczy P, Horn P, Thome C, Munch E, Schmiedek P. Regional cerebral blood flow monitoring in the diagnosis of delayed ischemia following aneurysmal subarachnoid hemorrhage. J Neurosurg 2003;98:1227–1234. [PubMed: 12816269]

Westermaier T, Jauss A, Eriskat J, Kunze E, Roosen K. Time-course of cerebral perfusion and tissue oxygenation in the first 6 h after experimental subarachnoid hemorrhage in rats. J Cereb Blood Flow Metab 2009;29:771–779. [PubMed: 19156162]

Yatsushige H, Calvert JW, Cahill J, Zhang JH. Limited role of inducible nitric oxide synthase in blood-brain barrier function after experimental subarachnoid hemorrhage. J Neurotrauma 2006;23:1874–1882. [PubMed: 17184195]

Yatsushige H, Ostrowski RP, Tsubokawa T, Colohan A, Zhang JH. Role of c-Jun N-terminal kinase in early brain injury after subarachnoid hemorrhage. J Neurosci Res 2007;85:1436–1448. [PubMed: 17410600]

Zuccarello M, Kassell NF, Sasaki T, Fujiwara S, Nakagomi T, Lehman RM. Barrier disruption in the major cerebral arteries after experimental subarachnoid hemorrhage in spontaneously hypertensive and normotensive rats. Neurosurgery 1987;21:515–522. [PubMed: 3683785]

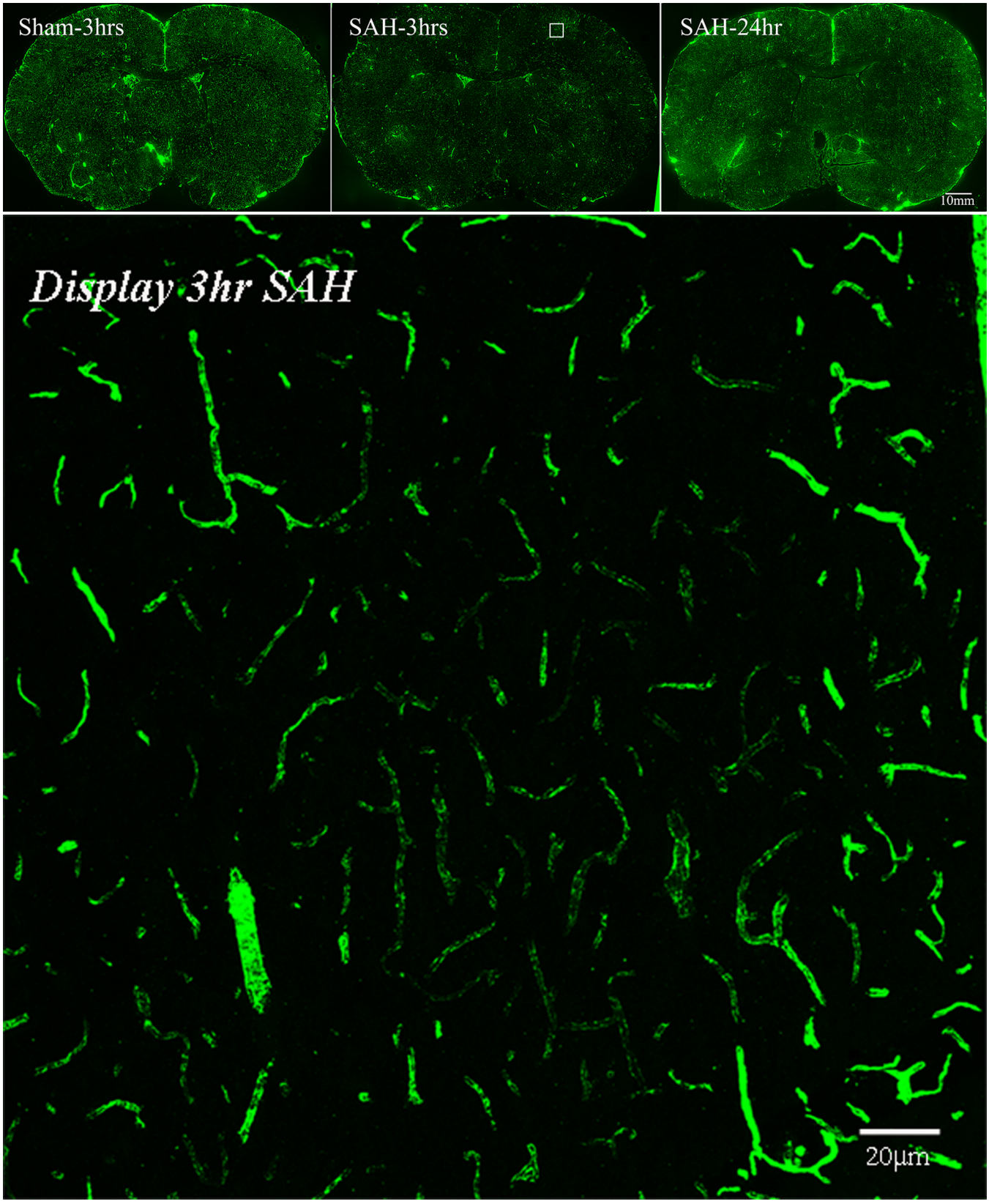

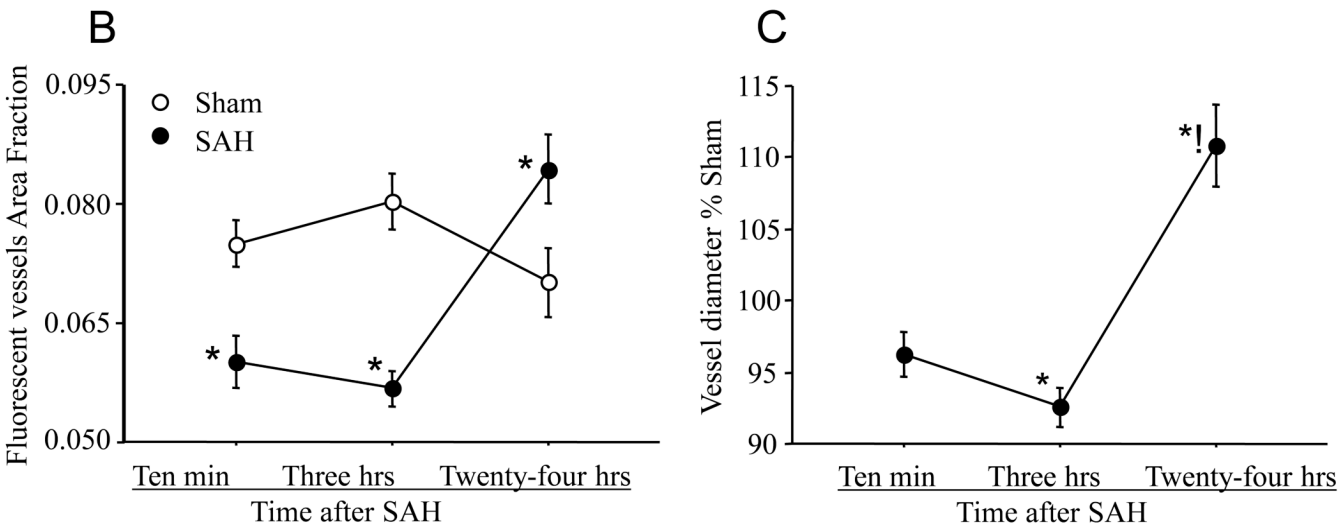

Figure-1. Perfusion deficits in parenchymal vessels after SAH

Animals were sacrificed at 10 minutes, 3 or 24 hours after Sham or SAH surgeries. Perfusion was visualized as the vascular presence of FITC-dextran injected 10 seconds before sacrifice. A: representative coronal brain sections from animals sacrificed at 3 hours after sham or 3 or 24 hours after SAH surgeries. Note the decrease in FITC-dextran labeled vessels at 3 hours after SAH and an increase at 24 hours as compared to sham. The boxed vessels in the in 3 hour SAH image are displayed in high magnification. B: Temporal change in area fraction of FITC-dextran positive vascular profiles during the first 24 hours after SAH. * significantly different than time matched sham cohorts at $P<0.05$. C: Temporal change in the diameter of FITC-dextran positive vascular profiles during the first 24 hours after SAH. Note small but significant increase in vessel diameter at 24 hour after SAH. Data are represented as % time matched shams. Mean ± sem, n=5 per time interval per surgery group. *: $P<0.05$.

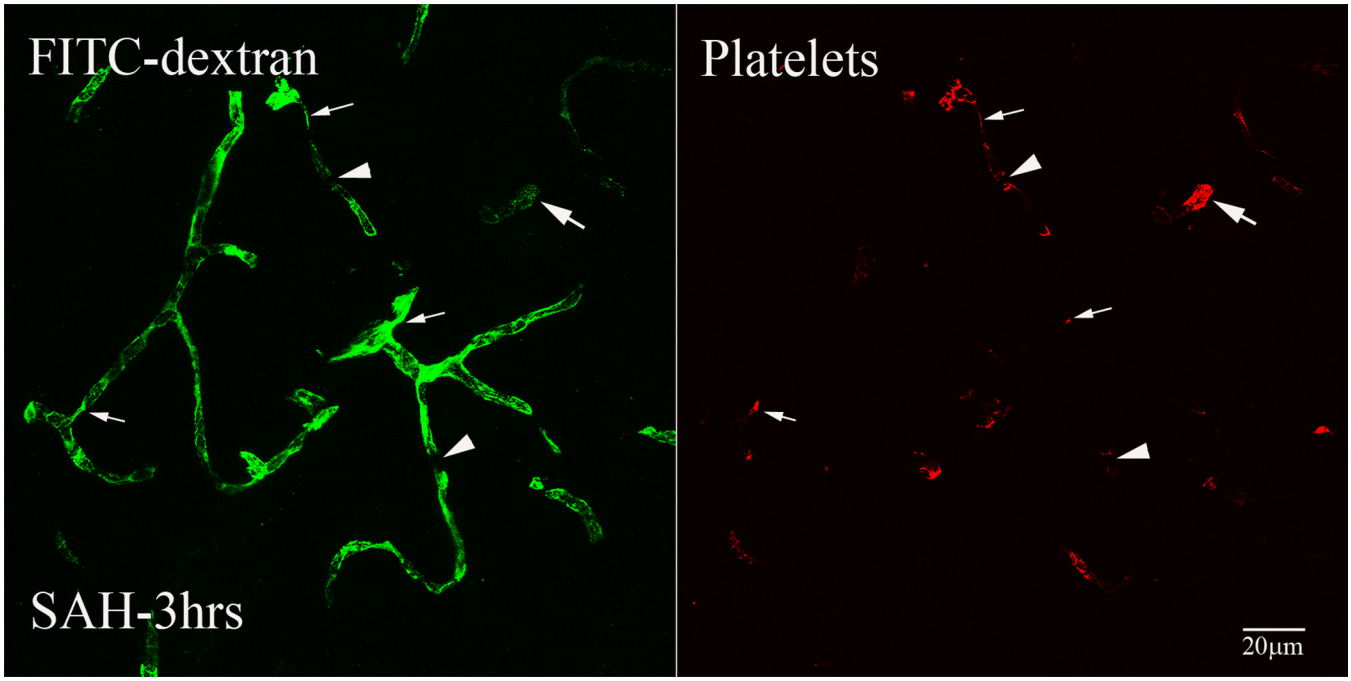

Figure-2. Intraluminal platelet aggregates contribute in perfusion deficits after SAH

Brain sections from FITC-dextran-injected animals were immunostained for platelets. Shown is a representative 3D rendered stacked high magnification image from animal sacrifice 3 hours after SAH. Two types of vascular segments could be seen; vascular segments filled with platelet aggregates but contain little FITC-dextran label *(arrows)* and vascular segments with decreased diameter filled with platelet aggregates and FITC-dextran *(thin arrows)*. Some FITC-dextran label vascular profiles appeared interrupted with platelet aggregates present at the interrupted edges *(arrow heads)*.

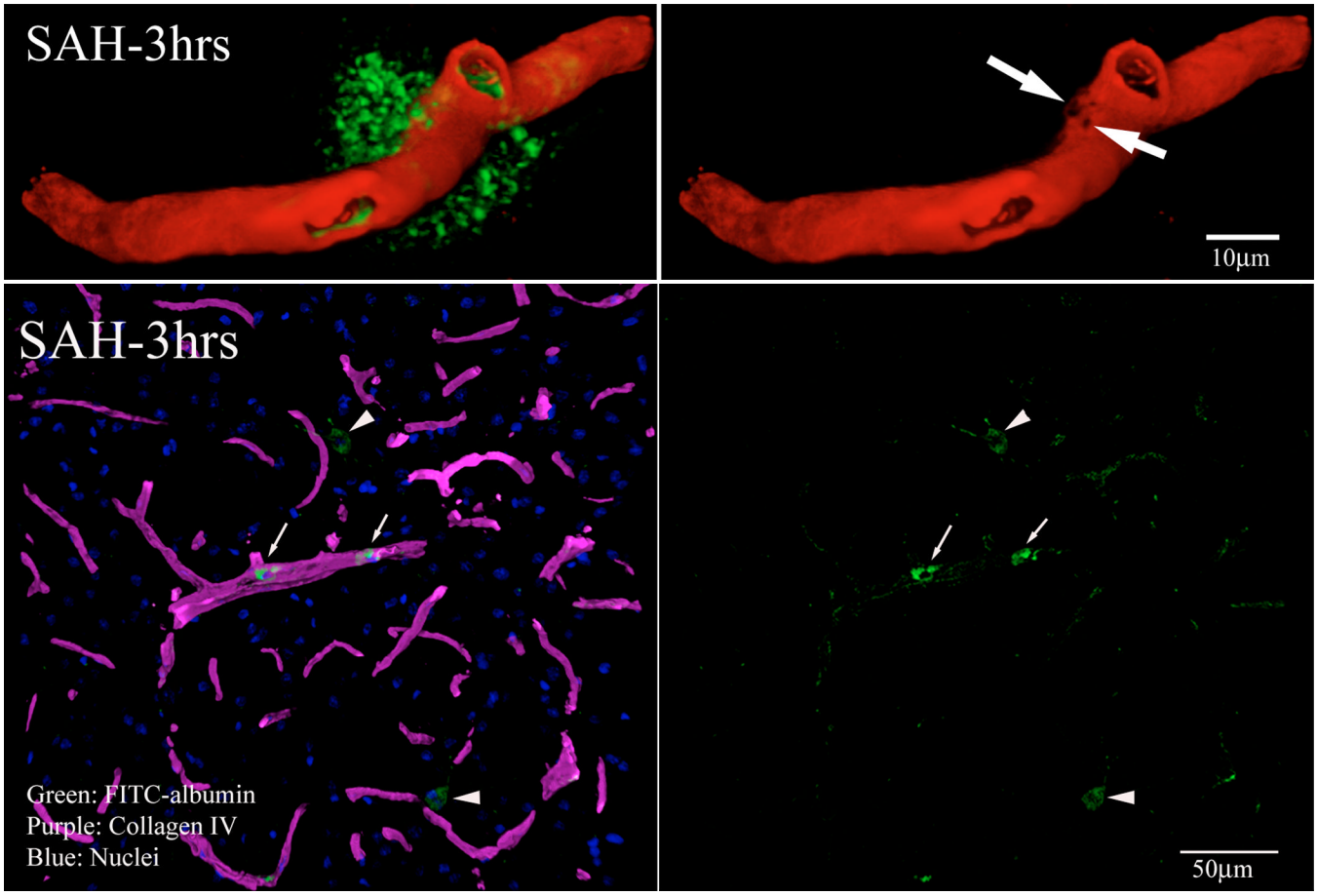

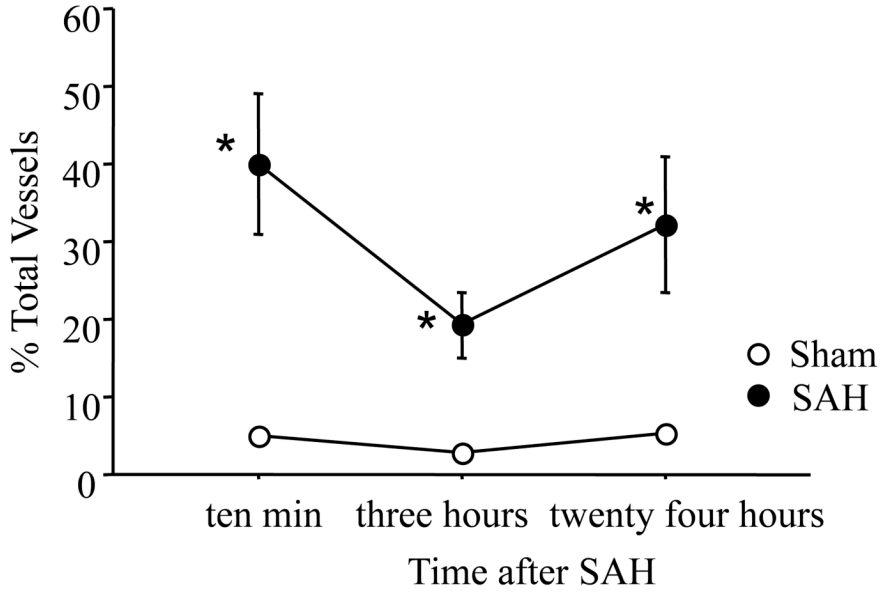

Figure 3C

Figure-3. Permeability changes in parenchymal vessels after SAH

Permeability was studied as extravasation of FITC-albumin injected 15 minutes before sacrifice. Brain sections were immunostained for collagen IV to delineate vessels. 3 D rendered stacked high magnification representative images from animals sacrificed 3 hours after SAH are shown. A: FITC-albumin leak from a collagen IV (red) immunostained vessel. B: A representative image showing green fluorescent vascular and parenchymal cells engaged in clean up process. Arrows: vascular green fluorescent cells, Arrow heads: parenchymal green fluorescent cells. C: FITC-albumin extravasation during the first 24 hours after SAH. Significantly greater number of vessels exhibited FITC-albumin extravasation at 10 minutes to 24 hours post-hemorrhage as compared to time matched sham cohorts. Data is representative as % time matched shams. Mean ± S.E.M, n=5 per time interval per surgery group. *: $P<0.05$.

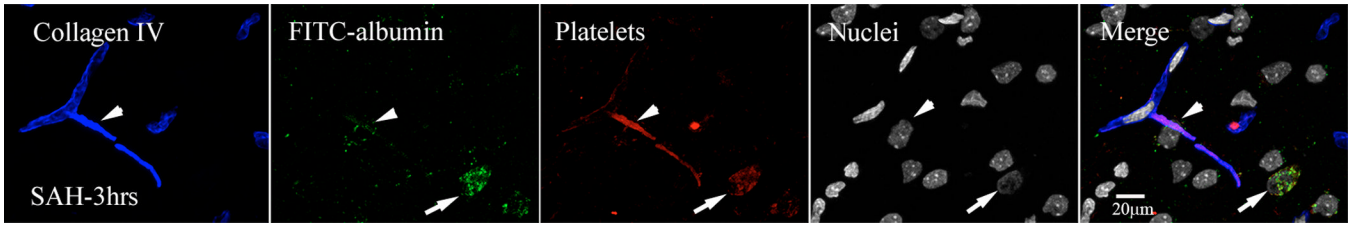

Figure-4. Intraluminal platelet aggregates contribute in permeability changes after SAH

FITC-albumin injected brains were immunostained for platelets and collagen IV. Shown is a representative high magnification image from animal sacrifice 3 hours after SAH. Arrow heads: extravasation of FITC-Albumin and platelet (red) form a single site on collagen (blue) immunostained vessel. Arrows: Also note green fluorescent cells engaged in vascular and parenchymal clean up process.